

Failure of feedback as a putative common mechanism of spreading depolarizations in migraine and stroke

Markus A. Dahlem, Felix M. Schneider, and Ekehard Schöll

Institut für Theoretische Physik, Technische Universität Berlin, Hardenbergstraße 36, D-10623 Berlin, Germany

The stability of cortical function depends critically on proper regulation. Under conditions of migraine and stroke a breakdown of transmembrane chemical gradients can spread through cortical tissue. A concomitant component of this emergent spatio-temporal pattern is a depolarization of cells detected as slow voltage variations. The velocity of ~ 3 mm/min indicates a contribution of diffusion. We propose a mechanism for spreading depolarizations (SD) that rests upon a nonlocal or non-instantaneous feedback in a reaction-diffusion system. Depending upon the characteristic space and time scales of the feedback, the propagation of cortical SD can be suppressed by shifting the bifurcation line, which separates the parameter regime of pulse propagation from the regime where a local disturbance dies out. The optimisation of this feedback is elaborated for different control schemes and ranges of control parameters.

During migraine and stroke neurological symptoms occur representing pathological events that spread through the cerebral cortex. While these clinical observations have been known for a long time, only recently direct measurements were made. Two studies have revealed common spatio-temporal wave patterns, one using functional magnetic resonance imaging in a migraine patient [1] and another using electrodes placed directly on the exposed cortical surface to record electrical activity in a stroke patient [2]. The observed spatio-temporal patterns in the cortex constitute examples of excitable behavior that evidently emerges from pathological pathways. Spatial systems that exhibit the emergent property that activity breaks away from a local stimulation site are called *excitable media* [3, 4]. The capacity to propagate pulses is the distinguishing feature of excitability in spatial systems. As a mechanism for shifting the onset of excitability in a reaction-diffusion system we propose failure of nonlocal or non-instantaneous feedback control.

I. INTRODUCTION

The propagation of pathological states is a particular aspect within the complex bidirectional relation between migraine and stroke [5]. Here we investigate this aspect, in particular, how cortical tissue when modeled as an excitable medium becomes susceptible to spreading events. Our knowledge about the mechanisms of propagation is still incomplete. It is generally believed that a common reaction-diffusion process, called *cortical spreading depression* (CSD) [6, 7, 8, 9, 10], captures essential features of the observed spreading phenomena during migraine and stroke. What makes cortical tissue susceptible to CSD has not been determined. Since the smooth lissencephalic cortex of animals is much more susceptible to CSD than the convoluted cortex of human, it was suggested that CSD in humans occurs very close to the

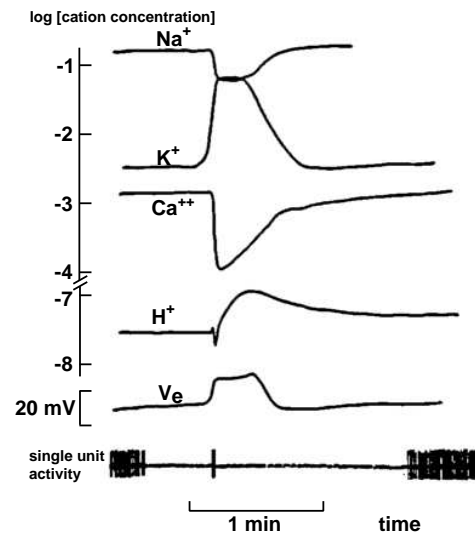


FIG. 1: Classical measurement of electrophysiological changes during cortical spreading depression [9]. Upper four traces: logarithmic representation of changes in Na^+ , K^+ , Ca^{++} , and H^+ concentration, lower two traces: extracellular potential shift V_e , and recording from a single neuron (single unit activity) vs. time. (Modified from [9])

onset of this emergent property [11, 12].

CSD is locally characterized by a nearly complete temporary breakdown of *ion homeostasis*, i. e., a stable stationary state (Fig. 1) [9]. Most electrophysiological changes follow a similar temporal course and return to normal after about one minute. A prominent signal is the slow negative potential shift V_e during CSD. It led to the term *spreading depolarization* (SD) to classify this and related phenomena as depolarization waves in the cerebral cortex [13]. Example of related phenomena are SD waves that contribute to progressive deterioration in regions surrounding an infarct core in stroke patients. These SD waves are called periinfarct depolariza-

tions (PID) [14]. We use the term SD for both cortical spreading depression and periinfarct depolarizations in this paper. In this terminology spreading depolarization is the more general term. The respective form of SD depends mainly on differences in the energy state of cortical tissue. In particular, differences between CSD and PID concern increased blood flow compensating the increased energy demands, which is typical for CSD occurring in healthy tissue during migraine but is reduced or missing in PID during stroke.

Differences in brain regions, e.g., concerning the cytoarchitecture or the distribution of ion channel types, also modify SD. We disregard the detailed pathophysiological characterization of the process, because it is still incompletely understood. Instead, in this study, SD is modeled with a standard reaction-diffusion system of activator-inhibitor type. Differences are reflected in the choice of the parameter values of the system. We extend the reaction-diffusion model by different kinds of local feedback signals. We propose that one way to think of such local feedback signals is in terms of control [15]. In this view, the feedback represents intrinsic cortical control mechanisms that reduce cortical susceptibility for CSD by stabilizing the physiological state of cortical tissue. Consequently, their failure under certain pathological conditions leads to the emergence of CSD, e.g., attributed to an underlying cortical hyperexcitability in migraine [16] or due to low energy levels in ischaemic tissue during stroke [14].

In this study, different feedback mechanisms with characteristic time and space scales are considered. Possible physiological basis of the feedback signals are motivated and discussed. We find that the excitability of the reaction-diffusion system can either increase or decrease. For each considered feedback scheme mainly the sign of the coupling strength determines whether feedback can suppress wave propagation, i.e., stabilize the homogeneous steady state of the tissue. A specific feedback scheme, in which activator and inhibitor variables are cross-coupled by non-local connections, indicates that opposed signs in the coupling strength for short-range and long-range connections are favorable for controlling the homogeneous steady state. This is a typical neuronal network connectivity pattern called *Mexican-hat connectivity*.

II. THE MODEL

While all evidence suggests that a reaction-diffusion process captures the essential features of SD, it is also clear that some features are oversimplified if we model SD with a standard reaction-diffusion mechanism of activator-inhibitor type. To create a more accurate albeit still generic model, we extend the standard reaction-diffusion model by a feedback mechanism. We introduce the feedback signal pathway in two variations. First, we introduce long-range connections as a spatial coupling in

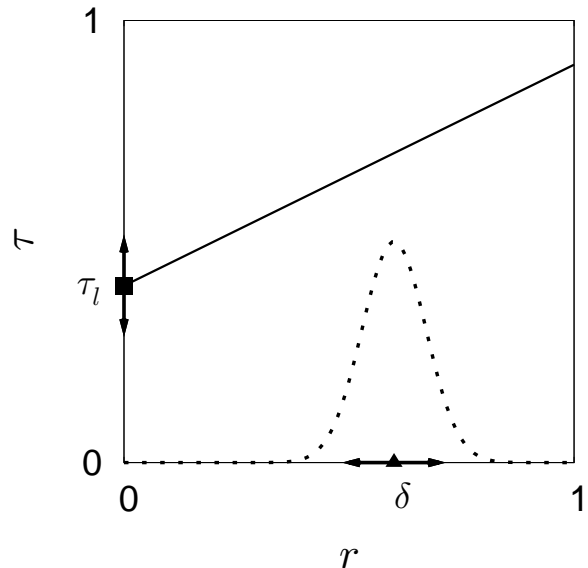


FIG. 2: Diagram of the spatial (r) and temporal (τ) characteristics (solid line) of the feedback signal, which is used to extend the FitzHugh-Nagumo (FHN) reaction-diffusion model. One of the two FHN variables is fed back via connections with length δ . The length is defined by the radial coordinate r of a local polar coordinate system, which lies parallel to the cortical surface and has its origin located where the connection terminates. Due to a finite propagation velocity c_s and a latency time τ_l of the feedback signal, a total time delay $\tau = \tau_l + c_s^{-1}\delta$ occurs. A kernel function $k(r)$ describes the spatial distribution of the connections, here exemplarily represented by a Gaussian (dashed). Two physiologically motivated limit cases of this general feedback type are considered: \blacktriangle instant feedback along long-range connections, and \blacksquare local time-delayed feedback.

addition to diffusion. This is motivated by the fact that high-frequency spikes in the population activity were observed up to millimeters ahead of the approaching front of SD [17, 18]. Second, we consider a localized time delayed feedback in the cortex, which can account for a slow feedback signal originating from the neurovascular coupling. Mathematically, these two extensions can be viewed as two limit cases of a general signal pathway (Fig. 2). Such a pathway serves as an additional coupling mechanism that is not included in a standard reaction-diffusion model. With this approach, we aim to describe universal features of excitable media modified by a feedback loop.

A. Reaction-Diffusion Model

We model the propagation of an initially localized breakdown of ion homeostasis in cortical tissue (Fig. 1) by an activator u and an inhibitor v as dynamic variables. They are coupled by kinetic reaction rates $f(u, v)$ and $g(u, v)$. We assume that only the activator species dif-

fuses in the medium. The equations are

$$\frac{\partial u}{\partial t} = f(u, v) + D\nabla^2 u \quad (1)$$

$$\frac{\partial v}{\partial t} = \epsilon g(u, v). \quad (2)$$

The parameter ϵ is the time scale ratio in the local dynamics of activator and inhibitor variables. The local spatial coupling is introduced by the diffusion term in Eq. (1) with the diffusion coefficient D . Without loss of generality, the value of D is normalized to unity. The choice of this value only scales the spatial coordinate.

In principle, there are two approaches to obtain the reaction rates $f(u, v)$ and $g(u, v)$. In a bottom-up approach, the reaction rates must be derived from a microscopic biophysical model of SD, where all major electrophysiological properties are represented. There is no consent so far on the mechanism of SD. Some models aim to provide a complete but rather local description of SD [19, 20, 21], that is, for processes occurring in a single neuron and its surrounding compartments. These models often introduce more than 20 dynamical variables. Therefore, a bottom-up approach with a subsequent reduction to two major activator and inhibitor agents seems not to be amenable. Nevertheless, it was shown that a two-species activator-inhibitor model can reproduce the spatio-temporal pattern of SD [11, 12, 22]. Even a reaction-diffusion model with a single species was successfully introduced for the purpose of an order-of-magnitude estimate of the expected propagation velocity of SD [7, 8]. Such calculations follow essentially a top-down approach, which we also adopt here. The basic activator-inhibitor mechanism, which we describe in the next paragraph, can be further expanded (top-down) to facilitate detailed investigation of further pathways and variables relevant to the study of specific questions concerning SD. Successful examples of such an approach are computational studies [23, 24] that supported a controversial hypothesis, namely that cortical tissue surrounding an infarct core dies because of the metabolic stress imposed by multiple SD waves.

The variables u and v assume the roles of activator and inhibitor, respectively. Their kinetic functions $f(u, v)$ and $g(u, v)$ are given by a cubic nonlinearity and a linear function, respectively,

$$f(u, v) = a\left(u - \frac{u^3}{3}\right) - v \quad (3)$$

$$g(u, v) = u - \beta - \gamma v \quad (4)$$

with parameters a , β , and γ . This is the FitzHugh-Nagumo (FHN) system, which is widely used as a generic model of excitable media [25, 26, 27]. Before we introduce the feedback, we compare the simulated spatial-temporal patterns with the ones observed during SD. In particular, the pulse profile and velocity in the FHN system are related to the corresponding quantities in SD (Fig. 1). Following this approach, we can estimate realistic values of the parameters of the FHN system.

B. FitzHugh-Nagumo system with feedback

To extend the standard FHN reaction-diffusion model we assume that a nonlocal feedback signal $s(x, y, t)$ is coupled back into the medium at any point (x, y) as

$$s(x, y, t) = K \int_0^{2\pi} \int_0^\infty k(r) (w(x + x_r, y + y_r, t - \tau) - w(x, y, t)) dr d\phi \quad (5)$$

where r and ϕ are the radius and the azimuthal angle, respectively, of a local polar coordinate system in (x, y) that lies parallel to the cortical surface, i. e., $x_r = r \cos \phi$, and $y_r = r \sin \phi$. The variable w may be chosen as either the activator u or the inhibitor v . The function $k(r)$ is the kernel function describing the spatial distribution of the pathway, which is typically peaked at a distance $r = \delta$, and K is the coupling strength. The parameter $\tau = \tau_p(r) + \tau_l$, with $\tau_p(r) = r/c_s$, is a time delay composed of a latency τ_l and a propagation delay τ_p . The latter is due to the finite signal propagation velocity c_s . A schematic diagram of the signal $s(x, y, t)$ is shown in Fig. 2. The feedback is, on the one hand, characterized by the parameter τ , and the kernel function $k(r)$, i. e., δ . We call this characterization the *type of coupling* of the feedback signal. On the other hand, there are two choices of w , namely the activator u and the inhibitor v . Furthermore, each type can either be fed back to the activator u or inhibitor v rate equation, i. e., Eq. (1) or Eq. (2), respectively. This allows for four different combinations, named *schemes*, two self-coupling and two cross-coupling schemes for each type of coupling. The two self-coupling schemes are referred to as “ uu ” if $w = u$ and “ vv ” if $w = v$, and the two cross-coupling schemes are referred to as “ uv ” if $w = u$ and “ vu ” if $w = v$. For example, in coupling scheme uu the activator is used to compose the feedback signal ($w = u$), which in turn is included in the activator rate equation (i. e., self-coupling). In a vector short-hand notation, the FHN system

$$\frac{\partial \zeta}{\partial t} = F(\zeta), \quad \text{with } \zeta = \begin{pmatrix} u \\ v \end{pmatrix} \quad (6)$$

is replaced by

$$\frac{\partial \zeta}{\partial t} = F(\zeta) + \sigma(x, y, t), \quad (7)$$

where the coupling is given by

$$\sigma = \begin{pmatrix} s \\ 0 \end{pmatrix}, \quad \text{or } \sigma = \begin{pmatrix} 0 \\ s \end{pmatrix} \quad (8)$$

with $w = u$ or $w = v$.

Note that we have constructed the nonlocal feedback signal (5) such that it contains the difference between the remote and local values of w . As a consequence, the signal $s(x, y, t)$ tends to zero if the pattern is homogeneous and stationary. The motivation for such a

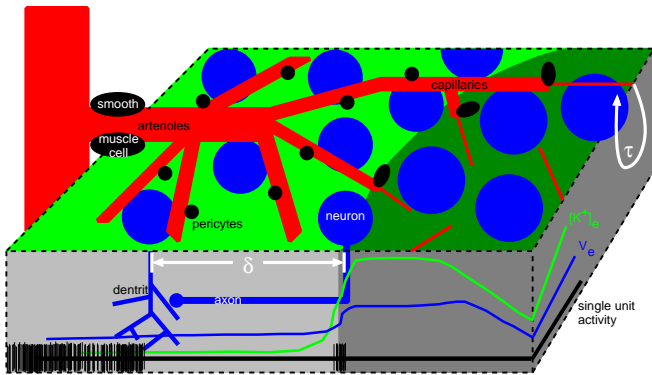


FIG. 3: Scheme of the cortical surface during cortical spreading depression. Red: blood vessels formed by endothelial cells. The cerebral blood flow starts at arterioles and leads to smaller capillaries, forming the capillary bed. Blue: neurons, green: glial cells. A pulse of cortical spreading depression moves from right to left, indicated by the shadowed region. The extracellular concentration changes of potassium $[K^+]_e$, the extracellular potential shift V_e , and the single unit activity are schematically related to the pulse on the lateral front surface. Note that the size of the different cells types are enlarged by about a factor of 10 in relation to these measured signals. The two considered feedback mechanisms are also illustrated: (i) long-range instantaneous lateral connections of length δ between neurons (shown on the lateral front surface), (ii) a time delayed feedback control (τ) of Pyragas type due to local response of the neurovascular unit (indicated on the right lateral side surface).

feedback is that this choice eliminates the feedback signal in the case of successful suppression of wave propagation. The signal $s(x, y, t)$ can be viewed as an intrinsic noninvasive control because it preserves the homogeneous steady state as the fixed point of the uncontrolled ($K = 0$) FHN system. In this way, it can be compared with the common time-delayed feedback control method introduced by Pyragas [28]. This method has been widely used with great success in problems in physics, chemistry, biology, and medicine [15] including reaction-diffusion systems [29, 30, 31, 32, 33]. In particular, it was demonstrated that it can be used to control the coherence and the timescales of noise-induced oscillations in a single FHN system [34, 35, 36] and in two coupled excitable FHN systems [37, 38] as well as noise-induced patterns in reaction-diffusion systems [39, 40, 41, 42] and wave propagation in excitable media [43]. This motivates our efforts to investigate whether a failure of such an intrinsic noninvasive control scheme can explain the onset of excitation spread in a spatially continuous FHN systems as a model of spreading pathological processes in the cortex during migraine and stroke.

1. Instant feedback along long-range connections

The first type of coupling that we consider is a limit case of Eq. (5). It is motivated by the observation of increased neuronal activity millimeters ahead of the approaching SD front. Although the cause and the effect of this activity remains unclear, it can be assumed that such activity is induced by SD via lateral cortical connectivity patterns (Fig. 3). In this case the signal propagation velocity c_s is several orders of magnitude faster than the velocity c of SD, i. e., $c_s \gg c$ ($50 \mu\text{m s}^{-1}$ in physical units). Consequently, the propagation delay τ_p can be neglected. Furthermore, the time scale of typical changes in electrophysiological activity is much faster than the time scale of changes due to the breakdown of ion homeostasis. The latter time scale is of the order of seconds (Fig. 1), which is also in agreement with our simulations of the FHN system if we dimensionalize the model equations (see section III below), while the former time scale, i. e., the delay due to chemical or electrical transmission at synapses, is of the order of milliseconds. Therefore, it is reasonable to assume that the latency τ_l of $s(x, y, t)$ is much smaller than the time scale of SD and that τ_l can also be neglected. This assumption can fail for metabotropic ion channels, like metabotropic glutamate receptors, which have increased open probabilities in the range of seconds after their activation. However, for ionotopically mediated activity we assume that $\tau_p \approx 0$ and $\tau_l \approx 0$, and therefore that the additional coupling signal $s(x, y, t)$ is, in this case, an instantaneous process ($\tau = 0$). Furthermore, we assume that the connectivity pattern is rather localized around the typical coupling length δ , and therefore, restricting ourselves to one spatial dimension, x , we approximate the kernel function by δ -functions $k(r) \approx \delta(x - \delta) + \delta(x + \delta)$. Taking these limits, Eq. (5) reduces to

$$s_\delta(x, t) = K(w(x - \delta, t) - 2w(x, t) + w(x + \delta, t)) \quad (9)$$

Note that Eq. (9) only in the limit $\delta \rightarrow 0$ becomes a standard diffusion term, however, for large δ , as considered here, it adds a novel type of nonlocal spatial coupling to the FHN model.

2. Local time-delayed feedback

The second type is also a limit case of Eq. (5). We consider a scenario that takes into account the coupling within the neurovascular unit. Therefore, it is particularly important for the dynamics of periinfarct depolarizations during stroke progression. The cerebral blood flow (CBF) is tightly regulated by the neurovascular unit to meet the brain's metabolic demands. These demands are extremely high during SD. The dynamics of the neurovascular unit are governed by various different cells types (Fig. 3). The interaction takes place between endothelial cells building the vessel walls, mural cells controlling vessel diameter, and glia and neurons. For the

purpose of our simplified scheme, that is, describing universal features of reaction-diffusion models of SD modified by an additional signal pathway, we concentrate on some key features of blood flow regulation that occur within the time and space scale given by a single passage of SD and that mimic the influence of the neurovascular unit.

The local CBF starts at arterioles, that is, blood vessels that extend and branch out from an artery and lead to capillaries. Capillaries are the smallest vessels, measuring $5 - 10\mu\text{m}$ in diameter. They form the capillary bed, a local network supplying the brain tissue. The CBF is regulated by two types of mural cells. Smooth muscle cells regulate arterioles, and pericytes regulate capillaries. The majority of the innervation of cerebral blood vessels terminate near capillaries suggesting that blood flow control is initiated in capillaries [44]. Therefore, we need to consider that increased activity during SD produces an initially localized hemodynamic response evoked by pericytes. To describe the action of the neurovascular unit on SD, the temporal and spatial distribution of the hemodynamic response needs to be considered.

First, we consider the spatial distribution of the hemodynamic response, which is determined by the vascular architecture. A precise spatial coordination of segmental vascular resistance is needed to effectively increase blood flow in a larger cortical area. Propagated vascular response signals are utilized to achieved this. It was shown that after the pericytes evoke a local capillary constriction, a pulse of constriction propagates at about $2\mu\text{m s}^{-1}$ to distant pericytes [44]. Furthermore, a dilatatory signal mediated by release of vasoactive agents propagates from metabolically active cells and evokes a remote response in upstream precapillary arterioles [45]. Considering the slow velocity of $2\mu\text{m s}^{-1}$ we can assume that global effects mediated by arterioles take place behind SD, i.e., after its passage, and therefore do not have a direct influence on the propagation of the wave front having passed. We assume that the response of the capillaries is rather localized, so that we can approximate the kernel function $k(x) \approx \delta(x)$. Consequently there is only a local response. Still there exists a latency delay τ_l due to slow metabolic effects when a local hemodynamic response is evoked by pericytes. Taking these limits, Eq. (5) now reduces to

$$s_\tau(x, t) = K(w(x, t - \tau) - w(x, t)), \quad (10)$$

which is identical with the noninvasive time-delayed feedback signal first introduced by Pyragas [28] for chaos control. This control method will now be applied to traveling pulses in excitable media. The latency delay time τ will be varied in our simulations.

Note that during stroke progression, the recruitment of periinfarct tissue into the infarct core is probably mediated by wave trains of periinfarct depolarizations [13]. Such periodic wave patterns are likely to be influenced by large scale hemodynamic responses. After the leading SD has initiated a slow propagating wave of constriction [44], subsequent waves in the wave train formation can be

influenced by this. This is beyond the scope of our study. To model a single SD pulse, we include the neurovascular unit by a localized time-delayed feedback signal $s_\tau(x, t)$ evoked from the change in blood flow which in turn is caused by pericytes in response to changes in neural activity.

III. RESULTS

It was suggested that SD in humans occurs close to the bifurcation of the onset of spreading activity in excitable media [11, 12]. Therefore, we first determine the location of this onset in the FHN system. Then we estimate the parameters of the FHN system from experimental data on SD (Fig. 1) and compare them with corresponding quantities in brain tissue. Finally, we investigate how the onset of excitability is influenced by the two types of coupling, $s_\delta(x, t)$ and $s_\tau(x, t)$, introduced in the previous section, in particular, how the onset is influenced by the newly introduced spatial and temporal scales δ and τ , respectively. To achieve this, we first consider the uncontrolled FHN system in the regime where sustained pulse propagation is possible and investigate whether or not the additional coupling schemes suppress pulse propagation. In this context, we can view the coupling scheme as a control scheme with the control goal to stabilize the homogeneous steady state [46, 47, 48]. Second, we choose parameter pairs (K_0, δ_0) and (K_0, τ_0) that suppress pulse propagation and determine the location of the onset of propagation in the FHN system with these coupling schemes. Furthermore, we determine the location of the onset of propagation in the FHN system for those cases where the coupling schemes cannot suppress pulse propagation.

1. Boundary of pulse propagation

The spread of an initially local activity arises in the system described by Eqs. (1)-(4) if a critical parameter value is crossed above which the medium is susceptible for sustained propagating excitation patterns [3, 49, 50, 51]. In a 1D medium this border is obtained by finding the regime where stationary solutions exist in a co-moving frame for specific activator and inhibitor profiles. In the co-moving frame $\xi = x + ct$, the coupled partial differential equations for activator and inhibitor variables Eq. (1)-(2) transform to a system of second order ordinary differential equations for $U(\xi)$ and $V(\xi)$

$$\begin{aligned} u(x, t) &= U(\xi) \\ v(x, t) &= V(\xi) \end{aligned} \quad (11)$$

which can be further transformed to a system of coupled first order ordinary differential equations of three variables, $U(\xi)$, $V(\xi)$, $W(\xi) \equiv \partial U(\xi)/\partial \xi$ [52]. Due to

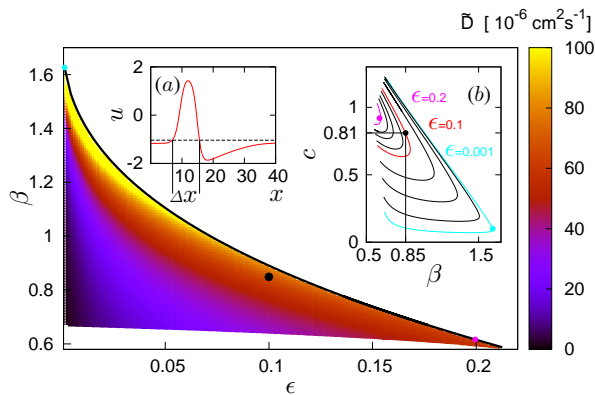


FIG. 4: Parameter space of the FHN system at $\gamma = 0.5$ and $a = 1$. The dimensionalized diffusion coefficient is color-coded as a function of the time scale ratio ϵ and the excitability threshold parameter β . The excitable regime (color-shaded) and the non-excitable regime (white) are separated by the boundary of propagation (thick black line). Above this boundary traveling pulse solutions do not exist. Inset (a) shows a typical pulse profile corresponding to the black dot in the main figure. Inset (b) shows homoclinic orbits of the FHN system in the co-moving frame with velocity c as a function of β for different values of ϵ . In this diagram, the location of the boundary of propagation is determined by the value of β at the turning point of each curve and the corresponding ϵ value, exemplarily shown by cyan and magenta dots for $\epsilon = 0.001$ and $\epsilon = 0.2$, respectively, in inset (b) and the main figure.

this transformation, c , the propagation velocity, is introduced as an additional parameter. In this system, homoclinic orbits can be found using a continuation method [53]. They correspond to travelling pulse solutions in Eq. (1)-(2) (Fig. 4, inset b). The transition into a region where homoclinic orbits exist marks a bifurcation of codimension one. In the parameter space of excitable media this bifurcation separates the regime supporting travelling pulses from the non-excitable regime. This border is shown in Fig. 4 in the parameter plane (ϵ, β) at the section $a = 1$ and $\gamma = 0.5$. As expected, the transition into the non-excitable regime is achieved by increasing either β or ϵ . Increasing β increases the threshold of the excitable medium, while increasing ϵ changes the time scale ratio between the dynamics of activator and inhibitor, with larger values of ϵ corresponding to faster inhibitor dynamics.

2. Estimate of space and time scales

The main reason to introduce spatial and temporal units in our FHN system is to obtain a better understanding of the typical values of the spatial and temporal coupling scales, δ and τ , respectively. Furthermore, the value of the diffusion coefficient D can be determined

if we introduce dimensional units in the FHN system. Note that D is not a bifurcation parameter. In the non-dimensionalized FHN system Eqs. (1)-(4), D can assume any value without changing the dynamics in a qualitative way. For example, changing D has no effect on the location of the propagation boundary shown in Fig. 4. Varying D is equivalent to scaling space units by $D^{-\frac{1}{2}}$. Therefore, the physical value of the diffusion coefficient D can be determined if we match the patterns obtained in the FHN system with the ones observed experimentally during SD.

First, we define characteristic space and time units, x_0 and t_0 , respectively. This is done with respect to the spatio-temporal patterns of the uncontrolled ($K = 0$) FHN system. These characteristic units are chosen such that the patterns calculated from the non-dimensionalized Eqs. (1)-(4) match the measured ones of Fig. 1. Introducing dimensional space (X) and time (T) variables by $x = X/x_0$ and $t = T/t_0$, the FHN system Eqs. (1),(2) assumes its dimensional form with the dimensionalized diffusion coefficient $\tilde{D} \equiv x_0^2/t_0$.

Now we compare the simulated pulse width Δx and duration Δt with the measured pulse width ΔX and measured duration ΔT (Fig. 1, $\Delta T \approx 20s$). Using the typical measured velocity of SD $C \approx 50\mu ms^{-1}$, we obtain $\Delta X = C\Delta T \approx 0.1cm$. The simulated pulse width Δx and duration Δt are related by $\Delta x = c\Delta t$ with the non-dimensionalized propagation velocity c , which appears as a parameter in Eq. (11) (e.g. for $\epsilon = 0.1$ and $\beta = 0.85$: $\Delta x \approx 8.7$ in Fig. 4 (inset a) and $c \approx 0.81$ in Fig. 4 (inset b), hence $\Delta t \approx 10.70$). Hence we infer the space and time units $x_0 = \Delta X/\Delta x \approx 115\mu m$ and $t_0 = \Delta T/\Delta t \approx 1.9s$, respectively, which yields a diffusion coefficient $\tilde{D} = x_0^2/t_0 \approx 70 \cdot 10^{-6}cm^2s^{-1}$, which is a reasonable value. Note that the pulse width Δx , the velocity c and hence x_0 , t_0 and \tilde{D} depend upon the parameters β and ϵ .

In Fig. 4 the obtained values for the diffusion coefficient \tilde{D} for each pair (ϵ, β) are shown in color coding. It ranges from $5 \cdot 10^{-6} - 100 \cdot 10^{-6}cm^2s^{-1}$ in the main part of the parameter space. As expected, low values are obtained in regions far away from the boundary of propagation. There the excitability of the system is high. On the other side, close to the propagation boundary, the values of \tilde{D} are higher. In this regime, the medium is weakly excitable or *subexcitable*. The correlation between the value of the obtained diffusion coefficients \tilde{D} and the excitability regimes requires some further clarification, which will be addressed in the discussion. However, note that the values of \tilde{D} in the parameter plane (ϵ, β) at the section $a = 1$ and $\gamma = 0.5$ are in the range of expected values for a diffusing substance participating in the mechanism of SD, as discussed in the literature [7, 8, 12, 54, 55].

3. Control of spreading depressions by $s_\delta(x,t)$ and $s_\tau(x,t)$

How does the additional coupling $s(x,t)$ change the FHN system? To answer this, we perform simulations with a variety of FHN systems in the parameter plane (ϵ, β) at $a = 1$ and $\gamma = 0.5$. The systems are chosen close to the propagation boundary (Fig. 4). We include both types of coupling, the instant feedback along long-range connections $s_\delta(x,t)$, described in section II.1, and the local time-delayed feedback $s_\tau(x,t)$, described in section II.2. Both types are considered separately. For each type of coupling there are four coupling schemes, two self-coupling schemes (uu, vv) and two cross-coupling schemes (uv, vu).

To obtain the influence of the coupling schemes on the FHN system, we start each individual simulation with a stable pulse profile of the reaction-diffusion system obtained without the coupling signal ($K = 0$). Then, for $K \neq 0$, we determined whether or not the pulse propagation is terminated. If the propagation is suppressed, we also determine how long the pulse can still propagate before it disappears. This distance defines the volume of tissue at risk (TAR), referring to the risk of cortical tissue surrounding a local pathological core of being recruited into the disturbed state [56]. This TAR value is taken as a measure of the efficiency of the coupling scheme as a control method.

First, we consider the four non-local schemes in $s_\delta(x,t)$, i. e., instant coupling along long-range connections (Sec. II.1). Regions in which pulse propagation is suppressed are shown in Fig. 5 a-d. The TAR value is given by a color code in this regions. For the two cases where we introduce self-coupling (Fig. 5 a ($w = u$) and d ($w = v$)), mainly the sign of the coupling constant K determines the success of the coupling scheme. Pulse propagation cannot be suppressed with negative values of K . This can be intuitively understood, if we consider only the effect of the signal $s_\delta(x,t)$ on the homogeneous steady state. A small disturbance from the homogeneous state is destabilized by $s_\delta(x,t)$ if $K < 0$ and stabilized if $K > 0$. Optimal values of δ are obtained for $w = u$ at $\delta \approx \Delta x$ and for $w = v$ at $\delta \approx 0.5\Delta x$. The picture changes for the two schemes with cross-coupling (Fig. 5 b ($w = v$) and c ($w = u$)). Successful suppression of pulse propagation in these cases depends on both the coupling strength K and the coupling length δ . The change in the sign of K occurs at $\delta \approx \Delta x$. If $\delta < \Delta x$, K must be positive (negative) if the coupling term $s_\delta(x,t)$ is fed into the inhibitor (activator) balance equation Eq. (2) or (1), respectively, and vice versa for $\delta \Delta x$. In other words, the short and long range control domains have opposite signs of K . Optimal values of δ in the short range control domain are obtained at $\delta \approx 0.5\Delta x$.

Next, we consider the local time-delayed feedback coupling (Sec. II.2). In each of the four coupling schemes control is only achieved if K is either positive or negative (Fig. 5 e-h). For positive K , the pulse propagation is suppressed if the signal is coupled into the activator u .

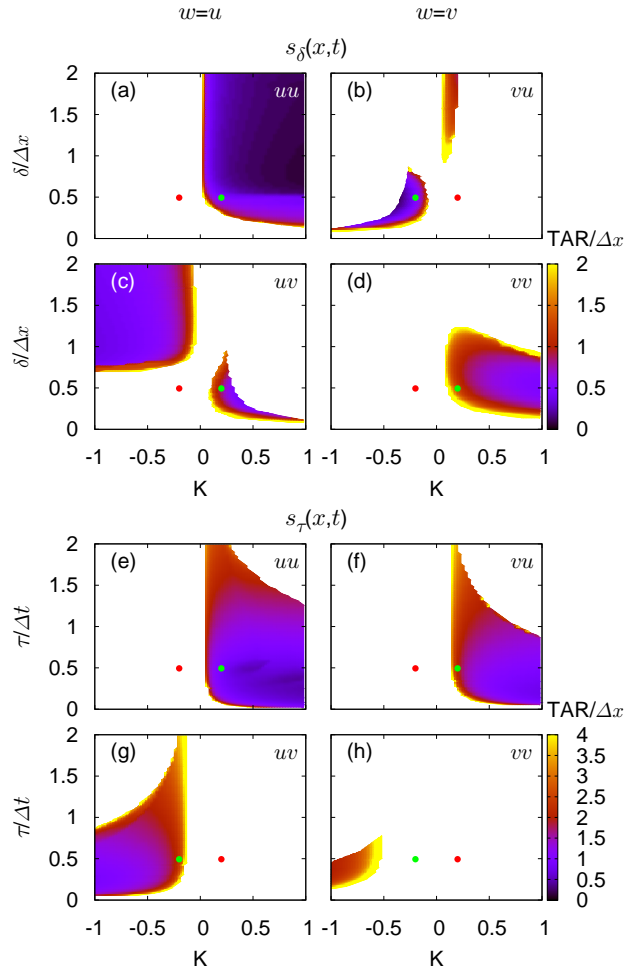


FIG. 5: Control planes for the four coupling schemes of the two types of feedback $s_\delta(x,t)$ (a-d) and $s_\tau(x,t)$ (e-h). (a,e): self-coupling of the activator signal (uu); (b,f): self-coupling of the inhibitor signal (vv); (c,g): cross-coupling with the feedback signal composed of the activator ($w = u$) and fed back to the inhibitor rate equation (w); (d,h): cross-coupling with the inverse configuration as compared to (c,g), i. e., (vu). The parameter values of the FHN system are $\epsilon = 0.1$, $\beta = 0.85$, $a = 1$, and $\gamma = 0.5$. This system is close to the propagation boundary (see black dot in Fig. 4). Regions in which pulse propagation is suppressed by the feedback signal are shown color coded by the tissue at risk (TAR) value, that is, the volume of tissue recruited into the pathological state before the pulse dies out. Low TAR values indicate that the feedback signal is more efficient. Optimal values, i. e., low TAR values, for δ and τ are mainly located at about 0.5 times the activator pulse width and duration, respectively (see text). Red and green dots mark control parameter values (K, δ) and (K, τ) for which the shift in the pulse propagation boundary is calculated in Fig. 6.

The two domains in the (K, τ) plane, where pulse propagation is suppressed, are of comparable size (Fig. 5 e (self-coupling) and f (cross-coupling)). For negative K , the pulse propagation is suppressed if the signal is cou-

pled into the inhibitor v . In this case, the cross-coupling scheme (Fig. 5 g) has a domain of comparable size and shape as for cases shown in Fig. 5 e,f. The domain for the self-coupling scheme is much smaller with only large values of TAR, i. e., less efficient suppression of pulse propagation (Fig. 5 h). For all four cases, the optimal delay time is $\tau \approx 0.5\Delta t$.

4. Shift in the onset of excitability by $s_\delta(x, t)$ and $s_\tau(x, t)$

We now investigate the shift in the location of the propagation boundary (Fig. 4) caused by the four coupling schemes of both types of coupling $s_\delta(x, t)$ and $s_\tau(x, t)$. This boundary separates the excitable regime from the non-excitable regime. Intuitively it is clear that the suppression of pulses shifts the propagation boundary towards the excitable regime of the system with $K = 0$. If we consider the coupling schemes as control mechanisms, such a shift manifests itself as a successful control strategy that reduces the excitability of the system.

First, we consider the non-local type of coupling $s_\delta(x, t)$. The parameter values for $s_\delta(x, t)$ are set to $K = 0.2$ and $K = -0.2$, and $\delta = 0.5\Delta x$. For each of the four coupling schemes with $\delta = 0.5\Delta x$ only one value of K , either $K = 0.2$ or $K = -0.2$, suppresses pulse propagation (marked by green dots in Fig. 5). With this choice and depending upon the four coupling schemes, the control signal $s_\delta(x, t)$ lies either close to optimal δ values or on the opposite side, mirrored along the $K = 0$ axis (marked by red dots in Fig. 5), a location where the control goal is not achieved. In the cases of the two cross-coupling schemes, the value $K = -0.2$ for $w = v$ (Fig. 5 b) and the value $K = 0.2$ for $w = u$ (Fig. 5 c) lies in the center of the control domain with the short range connections. If we consider the four cases in which pulses are suppressed, the location of the propagation boundary is shifted into the excitable regime, indicated by differently colored regions in Fig. 6 a). It is evident that the uv and vu cross coupling schemes are most efficient. Note that for the least efficient coupling scheme (uu) the propagation boundary (edge of the green region in Fig. 6 a) is actually not shifted beyond the point $\epsilon = 0.1$ and $\beta = 0.85$ (black dot). This seems to be contradictory with the control domain shown in Fig. 5 a) but is consistent with the definition of the propagation boundary as a bifurcation line. Beyond this bifurcation line there do not exist any traveling pulse solutions, whereas Fig. 5 a) only states that a specific traveling pulse solution with a specific amplitude (the one of the uncontrolled system) is suppressed. This example illustrates the different nature of the information shown in Fig. 5 and Fig. 6. In the four cases with the opposite sign of the parameter value K , i. e., where pulses are not suppressed, the propagation boundary is shifted towards the non-excitable regime of the uncontrolled ($K = 0$) FHN system (dashed lines in Fig. 6 a).

Second, we consider the local, time-delayed type of

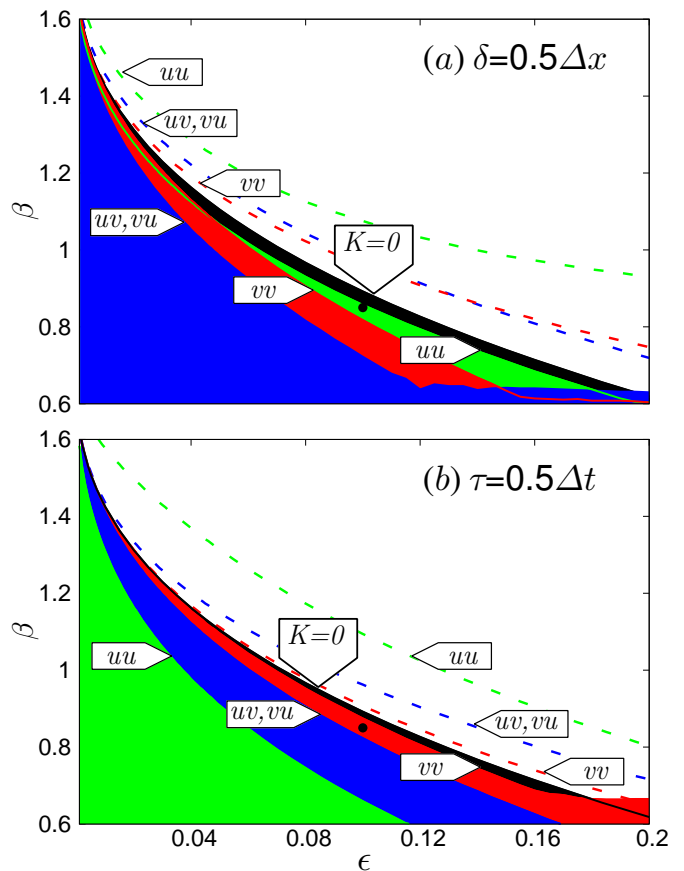


FIG. 6: Parameter space (ϵ, β) as in Fig. 4 showing excitable and non-excitable regimes for (a) non-local, (b) local time-delayed coupling. For the uncontrolled system ($K = 0$) the border between the excitable regime and the non-excitable regimes is between the black and white region. The other colored regions (green, red, blue) visualize the reduction of the excitable regime by the different coupling schemes as indicated by the location of the green dots in Fig. 5), i.e. K is chosen as $K = 0.2$ (uu , uv , vv in (a); uu , vu in (b)), or $K = -0.2$ (vu in (a); uv , vv in (b)). For each coupling scheme with opposite sign of K (red dots in Fig. 5) the excitable regime increases as indicated by the dashed lines.

coupling $s_\tau(x, t)$. The parameter values for $s_\tau(x, t)$ are set to $K = 0.2$ and $K = -0.2$, and $\tau = 0.5\Delta t$. To provide a comparison with the former type of coupling $s_\delta(x, t)$, we also choose the short range domain (as for $s_\delta(x, t)$ in Fig. 5 b,c) as the reference point and use these values of K also for $s_\tau(x, t)$. As before they are marked by green dots in Fig. 5 e,f,g if control is successful and red otherwise. Only for the scheme (vv) (Fig. 5 h) both types of coupling for $K = -0.2$ and $K = 0.2$ lie outside the control domain. Since the type with $K = -0.2$ is closer to a control domain, this is marked green, and correspondingly its propagation boundary is slightly pulled back as indicated by the red region in Fig. 6 b). Again we find a similar pattern as for the non-local type of coupling $s_\delta(x, t)$. The coupling schemes that suppress pulse propagation reduce excitability (colored regions in

Fig. 6 b) and the other ones increase excitability (dashed lines). Note that also for the coupling scheme (vv) transition occurs, with the only difference that the propagation boundary (edge of the red region in Fig. 6 b) is not shifted beyond the point $\epsilon = 0.1$ and $\beta = 0.85$ (black dot), which is in agreement with the control domain shown in Fig. 5 g.

DISCUSSION AND CONCLUSIONS

We have shown that a weakly excitable reaction-diffusion system can be shifted across the boundary of pulse propagation (Fig. 6) by various types of feedback and coupling schemes. In particular, we use non-local feedback $s_\delta(x, t)$ and time-delayed feedback $s_\tau(x, t)$. On the one hand, this is motivated by physiological considerations (Fig. 3). On the other hand, these two distinguished types allow for a clear separation of the effect of the introduced space scale δ and time scale τ upon the spatio-temporal pattern of SD. We have shown that these scales δ and τ are closely related. The reason is, of course, that the feedback is applied to control of travelling pulses. The velocity of SD relates space to time scales. Their numerical values can be compared after normalizing them with the pulse width Δx and pulse duration Δt , respectively. The common effect of both types of feedback on the traveling pulse is then reflected in the similar location of optimal control around half the pulse width and pulse duration for $s_\delta(x, t)$ and $s_\tau(x, t)$, respectively (Fig. 5). Therefore, the feedback mechanism, as given in a general form in Eq. (5), and illustrated in Fig. 2, provides a generic mechanism to modulate excitability in reaction-diffusion systems even if we consider only its two limit cases.

The reaction-diffusion system we have used to demonstrate the modulation of excitability by feedback is the FHN model. It represents excitable media exhibiting excitability of type II. Furthermore, we have constrained our investigations to the section $a = 1$ and $\gamma = 0.5$ in the four-dimensional parameter space of this model. Both restrictions, excitability of type II and this choice within the parameter space, will now be discussed. Type II excitability is related to a Hopf bifurcation, which is characterized by the fact that a periodic state bifurcates with a nonzero frequency [57]. Within an exponentially small range of either β or ϵ after the Hopf bifurcation a transition occurs, called *canard explosion*, from a state with small amplitude oscillations to a large amplitude relaxation oscillation. The canard explosion produces the threshold behavior (all-or-none) of the system needed to exhibit excitable behavior. Another typical bifurcation scenario leading to excitability is that the periodic state appears at a zero frequency [57, 58], called type I excitability. This can be modeled by a saddle-node bifurcation on a limit cycle or saddle-node infinite period bifurcation (SNIPER) [41, 59].

It is not clear which type of excitability is the ba-

sis of SD. However, experiments with retinal spreading depression indicate excitability of type II behavior [60]. The extracellular potassium concentration ($[K^+]_e$) was increased stepwise. Above a usually well preserved ceiling level of $[K^+]_e = 10\text{mM}$ [61] a rather spontaneous onset of oscillations with finite period was observed. Due to the presence of noise and a rather large step width of $\Delta[K^+]_e = 2\text{mM}$, a definite conclusion is not yet possible. However, we assume that our results hold in principle also for excitable media in which each local element is of excitability type I. The difference is manifest only close to the bifurcating state of the individual excitable element. In an excitable media, that is in a spatially extended system, excitability is defined by the distinguishing feature that the excited state breaks away from a local stimulated area due to transport, which usually involves diffusion. The bifurcating state of the individual elements seems therefore less important than the saddle-node bifurcation that leads to the emergence of traveling pulses (Fig. 4, inset b).

The FHN system is the most generic type that shows excitability of type II, because the activator equation, Eq. (1), has a cubic nonlinearity, which is generic for bistability [62, 63]. Since we aim to describe generic features, let us briefly comment on the choice of the two parameters that we have fixed ($a = 1$ and $\gamma = 0.5$). With this choice, the value of the diffusion coefficient in the main part of the remaining section of the parameter space is between $5 \cdot 10^{-6}\text{cm}^2\text{s}^{-1}$ and $100 \cdot 10^{-6}\text{cm}^2\text{s}^{-1}$ (Fig. 4). The diffusion coefficient of $[K^+]_e$, a substance often related to the activator or at least to the species by which SD propagates, is about $20 \cdot 10^{-6}\text{cm}^2\text{s}^{-1}$ in aqueous solution [64]. There are two counteracting effects that can significantly change this value in cortical tissue. First, due to the porous geometrical structure and small volume fraction of the extracellular space, which is similar to a soap phase, the apparent diffusion coefficient of $[K^+]_e$ in brain tissue is estimated to $7.2 \cdot 10^{-6}\text{cm}^2\text{s}^{-1}$ [54]. Second, the possibility that $[K^+]_e$ enters glial cells in one place and leaves elsewhere provides a form of facilitated diffusion that is estimated to be up to five times more important than diffusion in the extracellular space [8]. In summary, a generic model that simulates traveling pulses with a diffusion coefficient \tilde{D} of reasonable order of magnitude seems to be appropriate.

We propose that a failure of feedback provides a common mechanism of the emergence of spreading depolarizations in migraine and stroke. A recent study taking a complementary bottom-up approach, by describing SD in a detailed biophysical model, has concluded that the key to normal stability of cortical tissue is the effective regulation of $[K^+]_e$ by the neuron's Na-K ion pump and the glia-endothelial system [20]. This complements our conclusions. In our generic approach, our concern is not to identify the precise species behind activator, inhibitor, and feedback signals, but rather to describe spatial properties of their interaction and the emergence of travelling pulses. On the contrary, a detailed biophysical model of

properties of a single neuron and its surrounding extracellular compartments can only infer statements about the local excitable state. Whether a local breakdown of ion and transmitter homeostasis recruits further tissue into the excitable state or remains restricted to the initial focus is the clinically important question. This can only be answered in an extended system with sufficient spatial resolution, where a pulse propagation boundary can be defined (Fig. 4). The existence of the propagation boundary has consequences for therapeutic approaches that aim at an effective reduction of excitability to hold

the tissue below the bifurcating state and with that limit the tissue at risk [56].

Acknowledgements

This work was supported by DFG in the framework of Sfb 555. The authors would like to thank H. Engel, H. R. Wilson, and K. Showalter for fruitful discussions.

-
- [1] N. Hadjikhani, M. Sanchez Del. Rio., O. Wu, D. Schwartz, D. Bakker, B. Fischl, K. K. Kwong, F. M. Cutrer, B. R. Rosen, R. B. Tootell, A. G. Sorensen, and M. A. Moskowitz: *Mechanisms of migraine aura revealed by functional MRI in human visual cortex*, Proc. Natl. Acad. Sci. USA **98**, 4687 (2001).
- [2] M. Fabricius, S. Fuhr, R. Bhatia, M. Boutelle, P. Hashemi, A. J. Strong, and M. Lauritzen: *Cortical spreading depression and peri-infarct depolarization in acutely injured human cerebral cortex*, Brain **129**, 778 (2006).
- [3] A. T. Winfree: *Varieties of spiral wave behaviour: An experimentalist's approach to the theory of excitable media*, Chaos **1**, 303 (1991).
- [4] A. S. Mikhailov and K. Showalter: *Control of waves, patterns and turbulence in chemical systems*, Phys. Rep. **425**, 79 (2006).
- [5] M. G. Boussier and K. M. Welch: *Relation between migraine and stroke*, Lancet Neurol **4**, 533 (2005).
- [6] A. A. P. Leão: *Spreading depression of activity in the cerebral cortex*, J. Neurophysiol. **7**, 359 (1944).
- [7] B. Grafstein: *Neural release of potassium during spreading depression.*, in *Brain Function. Cortical Excitability and Steady Potentials.*, edited by M. A. B. Brazier (University of California Press, Berkeley, 1963), pp. 87–124.
- [8] A. R. Gardner-Medwin: *Possible roles of vertebrate neuroglia in potassium dynamics, spreading depression and migraine*, J. Exp. Biol. **95**, 111 (1981).
- [9] M. Lauritzen: *Pathophysiology of the migraine aura. The spreading depression theory*, Brain **117**, 199 (1994).
- [10] H. Martins-Ferreira, M. Nedergaard, and C. Nicholson: *Perspectives on spreading depression*, Brain. Res. Brain Res. Rev. **32**, 215 (2000).
- [11] M. A. Dahlem and E. P. Chronicle: *A computational perspective on migraine aura*, Prog. Neurobiol. **74**, 351 (2004).
- [12] M. A. Dahlem and S. C. Müller: *Reaction-diffusion waves in neuronal tissue and the window of cortical excitability*, Ann. Phys. **13**, 442 (2004).
- [13] J. P. Dreier, J. Woitzik, M. Fabricius, R. Bhatia, S. Major, C. Drenckhahn, T.-N. Lehmann, A. Sarrafzadeh, L. Willumsen, J. A. Hartings, O. W. Sakowitz, J. H. Seemann, A. Thieme, M. Lauritzen, and A. J. Strong: *Delayed ischaemic neurological deficits after subarachnoid haemorrhage are associated with clusters of spreading depolarizations*, Brain **129**, 3224 (2006).
- [14] K. A. Hossmann: *Periinfarct depolarizations*, Cerebrovasc. Brain Metab. Rev. **8**, 195 (1996).
- [15] E. Schöll and H. G. Schuster (Editors): *Handbook of Chaos Control* (Wiley-VCH, Weinheim, 2008), second completely revised and enlarged edition.
- [16] K. M. Welch: *Brain hyperexcitability: the basis for antiepileptic drugs in migraine prevention*, Headache **45**, 25 (2005).
- [17] O. Herreras, C. Largo, J. M. Ibarz, G. G. Somjen, and R. Martin del Rio: *Role of neuronal synchronizing mechanisms in the propagation of spreading depression in the in vivo hippocampus*, J. Neurosci. **14**, 7087 (1994).
- [18] B. Larrosa, J. Pastor, L. Lopez-Aguado, and O. Herreras: *A role for glutamate and glia in the fast network oscillations preceding spreading depression*, Neuroscience **141**, 1057 (2006).
- [19] H. C. Tuckwell and R. M. Miura: *A mathematical model for spreading cortical depression*, Biophysical J. **23**, 257 (1978).
- [20] H. Kager, W. J. Wadman, and G. G. Somjen: *Simulated seizures and spreading depression in a neuron model incorporating interstitial space and ion concentrations*, J. Neurophysiol. **84**, 495 (2000).
- [21] B. E. Shapiro: *Osmotic forces and gap junctions in spreading depression: a computational model*, J. Comput. Neurosci. **10**, 99 (2001).
- [22] J. A. Reggia and D. Montgomery: *A computational model of visual hallucinations in migraine*, Comput. Biol. Med. **26**, 133 (1996).
- [23] K. Revett, E. Ruppin, S. Goodall, and J. A. Reggia: *Spreading depression in focal ischemia: a computational study.*, J. Cereb. Blood Flow Metab. **18**, 998 (1998).
- [24] E. Ruppin, K. Revett, E. Ofer, S. Goodall, and J. A. Reggia: *Penumbra tissue damage following acute stroke: a computational investigation*, Prog. Brain Res. **121**, 243 (1999).
- [25] R. FitzHugh: *Impulses and physiological states in theoretical models of nerve membrane*, Biophys. J. **1**, 445 (1961).
- [26] J. Nagumo, S. Arimoto, and S. Yoshizawa.: *An active pulse transmission line simulating nerve axon.*, Proc. IRE **50**, 2061 (1962).
- [27] B. Lindner, J. García-Ojalvo, A. Neiman, and L. Schimansky-Geier: *Effects of noise in excitable systems*, Phys. Rep. **392**, 321 (2004).
- [28] K. Pyragas: *Continuous control of chaos by self-controlling feedback*, Phys. Lett. A **170**, 421 (1992).
- [29] O. Beck, A. Amann, E. Schöll, J. E. S. Socolar, and

- W. Just: *Comparison of time-delayed feedback schemes for spatio-temporal control of chaos in a reaction-diffusion system with global coupling*, Phys. Rev. E **66**, 016213 (2002).
- [30] N. Baba, A. Amann, E. Schöll, and W. Just: *Giant improvement of time-delayed feedback control by spatio-temporal filtering*, Phys. Rev. Lett. **89**, 074101 (2002).
- [31] J. Unkelbach, A. Amann, W. Just, and E. Schöll: *Time-delay autosynchronization of the spatiotemporal dynamics in resonant tunneling diodes*, Phys. Rev. E **68**, 026204 (2003).
- [32] J. Schlesner, A. Amann, N. B. Janson, W. Just, and E. Schöll: *Self-stabilization of high frequency oscillations in semiconductor superlattices by time-delay autosynchronization*, Phys. Rev. E **68**, 066208 (2003).
- [33] J. Schlesner, V. Zykov, H. Engel, and E. Schöll: *Stabilization of unstable rigid rotation of spiral waves in excitable media*, Phys. Rev. E **74**, 046215 (2006).
- [34] N. B. Janson, A. G. Balanov, and E. Schöll: *Delayed feedback as a means of control of noise-induced motion*, Phys. Rev. Lett. **93**, 010601 (2004).
- [35] A. G. Balanov, N. B. Janson, and E. Schöll: *Control of noise-induced oscillations by delayed feedback*, Physica D **199**, 1 (2004).
- [36] T. Prager, H. P. Lerch, L. Schimansky-Geier, and E. Schöll: *Increase of coherence in excitable systems by delayed feedback*, J. Phys. A **40**, 11045 (2007).
- [37] B. Hauschildt, N. B. Janson, A. G. Balanov, and E. Schöll: *Noise-induced cooperative dynamics and its control in coupled neuron models*, Phys. Rev. E **74**, 051906 (2006).
- [38] P. Hövel, M. A. Dahlem, and E. Schöll: *Synchronization of noise-induced oscillations by time-delayed feedback*, in *Proc. 19th Internat. Conf. on Noise and Fluctuations (ICNF-2007)* (American Institute of Physics, College Park, Maryland 20740-3843, 2007).
- [39] G. Stegemann, A. G. Balanov, and E. Schöll: *Noise-induced pattern formation in a semiconductor nanostructure*, Phys. Rev. E **71**, 016221 (2005).
- [40] G. Stegemann, A. G. Balanov, and E. Schöll: *Delayed feedback control of stochastic spatiotemporal dynamics in a resonant tunneling diode*, Phys. Rev. E **73**, 016203 (2006).
- [41] J. Hizanidis, A. G. Balanov, A. Amann, and E. Schöll: *Noise-induced front motion: signature of a global bifurcation*, Phys. Rev. Lett. **96**, 244104 (2006).
- [42] J. Hizanidis and E. Schöll: *Control of noise-induced spatiotemporal patterns in superlattices*, phys. status solidi (c) **5**, 207 (2008).
- [43] A. G. Balanov, V. Beato, N. B. Janson, H. Engel, and E. Schöll: *Delayed feedback control of noise-induced patterns in excitable media*, Phys. Rev. E **74**, 016214 (2006).
- [44] C. M. Peppiatt, C. Howarth, P. Mobbs, and D. Attwell: *Bidirectional control of CNS capillary diameter by pericytes*, Nature **443**, 700 (2006).
- [45] C. Iadecola, G. Yang, T. J. Ebner, and G. Chen: *Local and propagated vascular responses evoked by focal synaptic activity in cerebellar cortex*, J. Neurophysiol. **78**, 651 (1997).
- [46] P. Hövel and E. Schöll: *Control of unstable steady states by time-delayed feedback methods*, Phys. Rev. E **72**, 046203 (2005).
- [47] S. Schikora, P. Hövel, H. J. Wünsche, E. Schöll, and F. Henneberger: *All-optical noninvasive control of unstable steady states in a semiconductor laser*, Phys. Rev. Lett. **97**, 213902 (2006).
- [48] T. Dahms, P. Hövel, and E. Schöll: *Control of unstable steady states by extended time-delayed feedback*, Phys. Rev. E **76**, 056201 (2007).
- [49] A. S. Mikhailov and V. S. Zykov: *Kinematical theory of spiral waves in excitable media: comparison with numerical simulations*, Physica D **52**, 379 (1991).
- [50] V. Hakim and A. Karma: *Theory of spiral wave dynamics in weakly excitable media: asymptotic reduction to a kinematic model and applications*, Phys. Rev. E **60**, 5073 (1999).
- [51] E. Mihaliuk, T. Sakurai, F. Chirila, and K. Showalter: *Feedback stabilization of unstable propagating waves*, Phys. Rev. E **65**, 065602 (2002).
- [52] Y. A. Kuznetsov: *Elements of Applied Bifurcation Theory* (Springer, New York, 1995).
- [53] E. J. Doedel, R. C. Pfaffenroth, A. R. Chambodut, T. F. Fairgrieve, Y. A. Kuznetsov, B. E. Oldeman, B. Sandstede, and X. Wang: *AUTO 2000: Continuation and Bifurcation Software for Ordinary Differential Equations (with HomCont)* (2006).
- [54] C. Nicholson and J. D. Phillips: *Ion diffusion modified by tortuosity and volume fraction in the extracellular microenvironment of the rat cerebellum*, J. Physiol. **321**, 225 (1981).
- [55] H. R. Wilson: *Spikes, Decisions, and Actions: The Dynamical Foundations of Neuroscience* (Oxford University Press, Oxford, 1999).
- [56] M. A. Dahlem, F. M. Schneider, and E. Schöll: *Efficient control of transient wave forms to prevent spreading depolarizations*, J. Theo. Biol. in print (2007).
- [57] G. B. Ermentrout: *Neural networks as spatio-temporal pattern-forming systems*, Rep. Prog. Phys. **61**, 353 (1998).
- [58] H. R. Wilson: *Simplified dynamics of human and mammalian neocortical neurons*, J. Theor. Biol. **200**, 375 (1999).
- [59] J. Hizanidis, R. Aust, and E. Schöll: *Delay-induced multistability near a global bifurcation*, Int. J. Bifur. Chaos (2008), in print (arXiv:nlin/0702002v2).
- [60] Y. A. Dahlem, M. A. Dahlem, T. Mair, K. Braun, and S. C. Muller: *Extracellular potassium alters frequency and profile of retinal spreading depression waves*, Exp. Brain Res. **152**, 221 (2003).
- [61] U. Heinemann and H. D. Lux: *Ceiling of stimulus induced rises in extracellular potassium concentration in the cerebral cortex of cat*, Brain Res **120**, 231 (1977).
- [62] E. Schöll: *Nonlinear spatio-temporal dynamics and chaos in semiconductors* (Cambridge University Press, Cambridge, 2001), Nonlinear Science Series, Vol. 10.
- [63] F. Schlögl: *Chemical reaction models for non-equilibrium phase transitions*, Z. Phys. **253**, 147 (1972).
- [64] R. H. Stokes: *The diffusion coefficients of eight uni-univalent electrolytes in aqueous solution at 25*, J. Am. Chem. Soc. **72**, 2243 (1950).